#### **OPTICS**

# Wavefront shaping enables high-power multimode fiber amplifier with output focus

Stefan Rothe<sup>1</sup>†, Chun-Wei Chen<sup>1,2</sup>†,Peyman Ahmadi<sup>1,3</sup>†, KyeoReh Lee<sup>1</sup>†, Kabish Wisal<sup>4</sup>, Mert Ercan<sup>1</sup>, Nathan Vigne<sup>1</sup>, A. Douglas Stone<sup>1</sup>, Hui Cao<sup>1</sup>\*

High-power fiber lasers are powerful tools used in science, industry, and defense. A major roadblock for further power scaling of single-frequency fiber laser amplifiers is stimulated Brillouin scattering. Efforts have been made to mitigate this nonlinear process, but these were mostly limited to single-mode or few-mode fiber amplifiers, which have good beam quality. Here, we explored a highly multimode fiber amplifier in which stimulated Brillouin scattering was greatly suppressed due to a reduction of light intensity in a large fiber core and a broadening of the Brillouin scattering spectrum by multimode excitation. By applying a spatial wavefront shaping technique to the input light of a nonlinear amplifier, the output beam was focused to a diffraction-limited spot. Our multimode fiber amplifier can operate at high power with high efficiency and narrow linewidth, which ensures high coherence. Optical wavefront shaping enables coherent control of multimode laser amplification, with potential applications in coherent beam combining, large-scale interferometry and directed energy delivery.

High-power lasers have enabled a wide range of applications such as laser machining, metrology, and directed energy delivery (1-4). The ultimate limit on power scaling of such lasers are the nonlinear effects and/or material damage encountered during light amplification inside the lasers. An important technique to overcome such detrimental effects in short-pulse amplifiers is chirped pulse amplification, in which laser pulses are stretched temporally, then amplified, and finally compressed (5). A similar technique for continuous-wave (CW) amplifiers is the spatial spread of light, for example, by increasing the core area of a fiber amplifier. However, a fiber of larger core tends to support more guided modes, and the interference of light in these modes will generate a pseudorandom spatial field distribution, leading to poor output beam quality. Because high beam quality is needed for many applications, there have been extensive efforts to increase the core area by reducing the numerical aperture (NA) (6-15) or to explore microstructured fibers while maintaining single-mode amplification (16). However, further power scaling is still limited by optical nonlinearities and instabilities [see the supplementary materials, section 3 (17)].

The lowest-power nonlinear limit in power scaling of narrow-band fiber amplifiers typically arises from stimulated Brillouin scattering (SBS) of light mediated by acoustic waves (18, 19). This effect scatters the forward-propagating signal to backward-propagating Stokes light, thus limiting the amplifier output power. Moreover, intense Stokes pulses might be generated that could damage upstream lasers. Various techniques have been developed to mitigate SBS, mostly in single-mode or few-mode fibers, to maintain high output-beam quality.

<sup>1</sup>Department of Applied Physics, Yale University, New Haven, CT, USA. <sup>2</sup>Edward L. Ginzton Laboratory, Stanford University, Stanford, CA, USA. <sup>3</sup>Coherent, Bloomfield, CT, USA. <sup>4</sup>Department of Physics, Yale University, New Haven, CT, USA. \*Corresponding author. Email: hui.cao@yale.edu †These authors contributed equally to this work.

One method used to increase the SBS threshold is to increase the signal linewidth to tens of gigahertz to effectively broaden the Brillouin scattering spectrum and thereby lower the peak gain for SBS (20). However, this approach greatly reduces temporal coherence, which is required for applications such as metrology and gravitational wave detection (21, 22). To suppress SBS in the single-frequency (linewidth <100 kHz) regime, different approaches have been explored [see the supplementary materials, section 3 (17)], such as tailoring acoustic and gain properties, applying differential strain and/or temperature gradients, tapering fiber core diameter, and tight coiling short fibers (10, 16, 23–30). However, SBS remains the major obstacle to power-scale, single-frequency, single-mode fiber (SMF) amplifiers (31).

Optical wavefront shaping has become a powerful technique for controlling light propagation in complex media including multimode fibers (MMFs) (32). For example, it has been found in previous studies that tailoring the incident wavefront of light to an MMF with a spatial light modulator (SLM) can create any spatial pattern of transmitted field that is a superposition of the fiber modes (33-35). However, most of these studies were conducted on passive MMFs with linear light propagation or on low-power MMF amplifiers with weak nonlinearity (36, 37). Adaptive mode control through a photonic lantern front end has been used to maintain single-mode operation in a few-mode fiber amplifier (38), but this scheme is difficult to extend to the highly multimode regime. Although large-scale wavefront shaping has been used to control nonlinear optical processes in passive MMFs (39-41), it has not been applied to high-power MMF amplifiers with strong nonlinearity, so its ability, efficacy, and robustness for controlling complex, unstable multimode amplification are not yet known.

Here, we simultaneously suppressed detrimental SBS and focused the output beam in a highly multimode nonlinear fiber amplifier using input wavefront shaping. Our MMF amplifier is free of SBS up to 503 W output power, which is ~30 times higher than the SBS limit in a standard SMF of same length. The slope efficiency is 82%, comparable to SMF amplifiers. The output of our MMF amplifier has a 20-dB linewidth of 18 kHz, corresponding to a 3-dB linewidth of 1 kHz. This linewidth is six orders of magnitude narrower than that of spectrally broadened SMF amplifiers, leading to six orders of magnitude longer temporal coherence length.

We addressed the main concern with using such an MMF amplifier, output beam quality, by focusing the output beam with input wavefront shaping. The beam propagation factor for the focal spot is  $M^2 \leq 1.35$ . The ability to control the output beam shape, together with the high temporal coherence of our MMF amplifier, will greatly facilitate coherent combining of output beams from multiple amplifiers.

#### **SBS**

In our master oscillator power amplifier configuration (Fig. 1), the linearly polarized CW output of a single-frequency laser oscillator at wavelength  $\lambda_{\rm S}=1064$  nm was preamplified by two-stage Yb-doped SMF preamplifiers. Using a liquid-crystal SLM, we applied phase-only modulation to the linearly polarized signal before coupling it to a Yb-doped MMF amplifier that supports 76 spatial modes. The doped fiber was cladding pumped by five diode lasers in the wavelength range of 966 to 971 nm to amplify the signal through stimulated emission of Yb ions [see the materials and methods for more details (17)].

In the fiber amplifier, the signal being amplified acted as a pump for SBS, generating a backward-propagating Stokes field by emitting forward-propagating acoustic waves. The Stokes field was amplified by both SBS and stimulated emission of excited Yb ions as it propagated backward through the fiber. With increasing pump power, the time trace of the backscattered light intensity showed random spikes of duration ~10 to 100 ns (left inset of Fig. 1). These sharp intensity fluctuations are attributed to an SBS-induced dynamic instability (42–45) and represent a precursor for the onset of SBS (19). Here, we

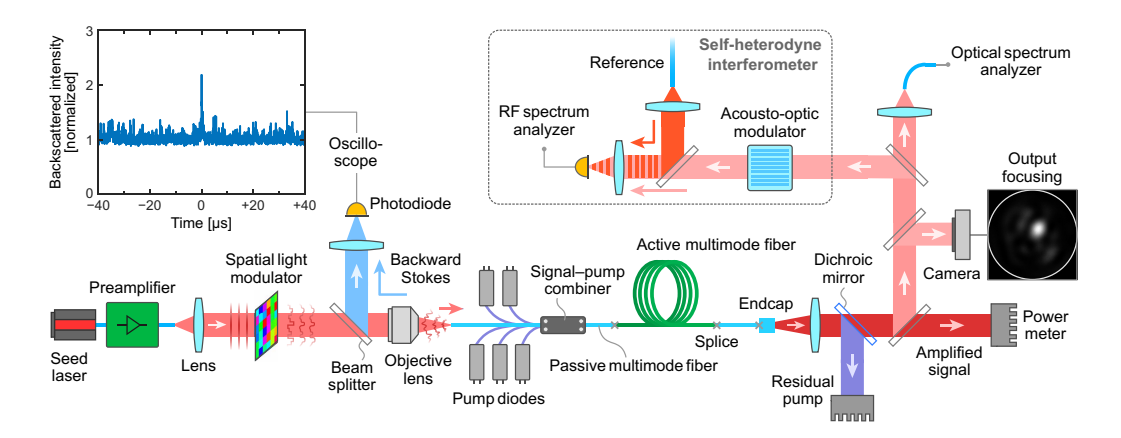


Fig. 1. Schematic of our MMF amplifier with input wavefront shaping to focus output beam. A single-frequency seed laser at wavelength  $\lambda_S = 1064$  nm was preamplified to 10 W. The CW beam was expanded and wavefront shaped by an SLM before coupling to a Yb-doped MMF amplifier pumped by five laser diodes. The amplified signal and residual pump were separated by a dichroic mirror, and their powers were measured by power meters. A camera recorded the near-field intensity distribution of the amplified signal outside of the MMF facet. The optical spectrum and linewidth of the output signal were measured with an optical spectrum analyzer and a heterodyne interferometer. The SLM shaped the input wavefront to focus the output beam to a diffraction-limited spot. The right inset shows the focal spot at an output power of 503 W. The left inset is the time trace of total backscattered intensity (normalized to its Rayleigh-scattering component), exhibiting a large spike due to SBS. RF, radiofrequency.

define the SBS instability threshold as the output signal power at which the maximum height of Stokes spikes is 1.5 times that of the continuous background from Rayleigh scattering in the backward intensity trace. This level is well below the conventional SBS threshold that is typically set by the condition that the reflected power equals a small percentage of the transmitted signal power (46).

Compared with the standard SMF amplifier, the large cross-section of our MMF amplifier lowers the signal intensity within the fiber core, thus reducing SBS. Similar to the conventional SBS threshold, the SBS instability threshold is expected to scale quadratically with the fiber core diameter [see the supplementary materials, section 2 (17)]. If only the fundamental mode (FM) was excited in our MMF with a 42-µm core, the SBS threshold was about eight times that in a large-mode-area SMF amplifier with a 15-µm core (19). From the previously measured SBS instability threshold in the SMF amplifier (45), we estimated the SBS instability threshold for FM-only excitation in our MMF ampifier to be 24 W, as shown in Fig. 2A.

Experimentally, it was difficult to realize FM-only excitation in the MMF amplifier because of the inevitable mode coupling in the fiber. When we used a lens of NA  $\approx 0.03$  to launch the signal into the MMF, the output beam was distorted from a smooth, symmetric profile (inset of Fig. 2A), indicating that both FM and a few high-order modes (HOMs) were excited. The measured SBS instability threshold for the few-mode excitation was 59 W. To excite more HOMs in the MMF amplifier, we replaced the lens with a microscope objective of NA = 0.13, slightly larger than the fiber NA = 0.1. With the input signal tightly focused onto the front facet of the MMF, the output beam was speckled, as seen in the inset of Fig. 2A. The measured SBS instability threshold for multimode excitation was 97 W.

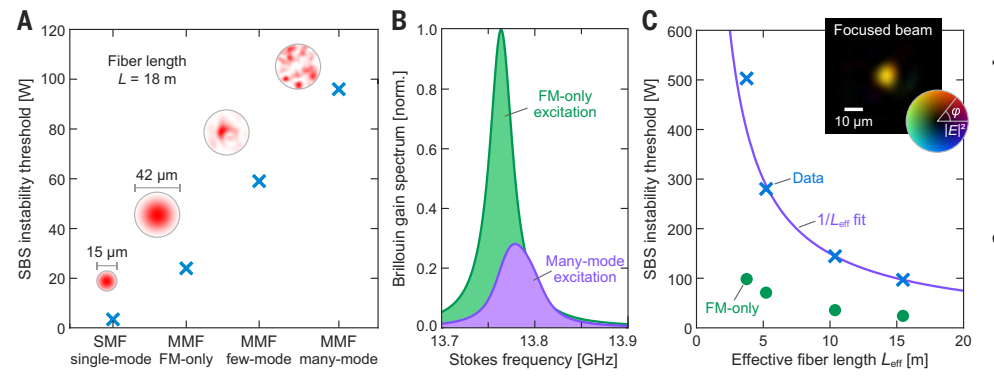


Fig. 2. SBS in single-frequency fiber amplifiers. (A) Output signal power at the SBS instability threshold estimated for a 15- $\mu$ m-core SMF amplifier and compared with a 42- $\mu$ m-core MMF amplifier under FM-only excitation. Inset shows the calculated intensity profile of the FM. SBS instability thresholds for the MMF amplifier were measured with few-mode and multimode excitations. Inset shows the output intensity distributions. Both SMF and MMF were 18 m long. (B) Brillouin gain spectrum calculated with equal excitation of all modes (purple) was broader than FM-only excitation (green) in the MMF amplifier. (C) SBS instability threshold as a function of effective fiber length  $1/L_{\rm eff}$  for the 42- $\mu$ m-core MMF with multimode excitation. Blue crosses are experimental data, and purple solid curve shows the  $1/L_{\rm eff}$  scaling. All data points were taken with the output beam focused to a diffraction-limited spot. Green circles represent the estimated SBS instability thresholds under FM-only excitation at corresponding lengths. The inset shows intensity and phase distributions across the focal spot at output signal power of 173 W. Seventy-six percent of total output power was concentrated inside the focus. Color represents phase and brightness represents the intensity.

#### Multimode SBS theory

The fourfold increase of the SBS instability threshold (24 to 97 W) by multimode excitation within the same MMF can be explained by our semianalytic theory of SBS in the MMF amplifier (46–48). When the input light is distributed over multiple fiber modes, the forward-propagating signal in each mode will be Brillouin scattered to backward-propagating Stokes in all modes. This process is mediated by acoustic modes in the fiber, and the Stokes is frequency downshifted from the signal by the acoustic frequency  $\Omega$ . The scattering coefficient for signal in the l-th mode and Stokes in the m-th mode,  $g_B^{(m,l)}(\Omega)$ , depends on the spatial overlap of the signal and Stokes mode profiles with various acoustic modes in the fiber. Each mode

pair of l and m typically has the largest spatial overlap with a single acoustic mode, meaning that  $g_B^{(m,l)}$  peaked at this acoustic mode frequency  $\Omega$ . The total Brillouin gain at axial position z in the m-th mode due to signals in all fiber modes is:

$$G_{\rm B}^{(m)}(z) = \sum_{l} g_{\rm B}^{(m,l)}(\Omega) P_{\rm S}^{(l)}(z)$$
 (1)

where  $P_{\rm S}^{(l)}$  is the signal power in the l-th mode. The growth rate of Stokes power in the m-th mode  $P_{\rm B}^{(m)}$  is determined by  $G_{\rm B}^{(m)}$ 

$$\frac{dP_{\rm B}^{(m)}}{-dz} = G_{\rm B}^{(m)} P_{\rm B}^{(m)}(z) \tag{2}$$

Because of the exponential nature of growth, the total Stokes power,  $P_{\rm B} = \sum_m P_{\rm B}^{(m)}$ , is dominated by the mode m that has the maximum value of  $G_{\rm B}^{(m)}$ .

 $G_B^{(m)}$  depends on the signal power distribution among the fiber modes. We consider three cases below. First, all of the signal power is in the FM, meaning l=1.  $g_B^{(l,l)}$  is larger than  $g_B^{(m,l)}$  for any m>1 because of better spatial overlap between optical and acoustic modes. Thus, Brillouin scattering is strongest for the Stokes field in the FM (m = 1), mediated by the lowest-order acoustic mode in the fiber. Second, consider when a single HOM l > 1 is excited. Because of larger acousto-optic overlap, intramodal Brillouin scattering (m = l) is stronger than intermodal scattering  $(m \neq l)$ ,  $g_B^{(l,l)} > g_B^{(m,l)}$  for any  $m \neq l$ . However, smaller acousto-optic overlap makes  $g_B^{(l,l)} < g_B^{(1,1)}$ , and the SBS threshold for l > 1 is higher than that with FM-only excitation. Third, if input power is distributed among all fiber modes, then  $G_B^{(m)}$  is a sum of intramodal and intermodal scattering coefficients weighted by the signal power  $P_{\rm S}^{(l)}$ in individual modes, which is much less than the total power. Because  $g_{\rm B}^{(m,l)}$  for different mode pairs peaked at varying frequencies  $\Omega$ ,  $G_{\rm B}^{(m)}$ is spectrally broadened and has a notably lower peak value than singlemode excitation (Fig. 2B). Because the peak value dictates the exponential growth of Stokes power, the SBS threshold is appreciably higher for multimode excitation than for the excitation of any single mode.

### Pump depletion and gain saturation

In a high-power MMF amplifier such as ours, gain saturation and pump depletion are strong. These effects determine the signal power distribution throughout the fiber, which affects the Stokes growth rate. To include these effects in our theory, we extended our earlier model (46) as follows. We first calculated the signal power in each mode  $P_S^{(l)}(z)$  throughout the fiber, taking into account gain saturation and pump depletion in the MMF amplifier (49). At or below the SBS instability threshold, the Stokes power is much lower than the signal power, so feedback due to SBS was neglected when computing the signal power and pump power distribution in the MMF amplifier [see the supplementary materials, section 2 (17)].

Numerical simulation of our MMF amplifier using the improved model [with parameters listed in table S1 (17)] revealed that the pump power (at wavelength  $\lambda_P=971$  nm) was mostly absorbed in the first 6 m of the Yb-doped fiber. Beyond this distance, the signal power did not grow appreciably [fig. S6 (17)]. To investigate the scaling of SBS instability threshold with fiber length, we started with a long fiber and gradually cut it back in Fig. 2C. From the physical fiber length L and total signal power  $P_{\rm S}(z)=\sum_{l}P_{\rm S}^{(l)}(z)$ , we computed the effective fiber length for SBS as follows:  $L_{\rm eff}=\int_{0}^{L}P_{\rm S}(z)dz/P_{\rm S}(L)$ . Figure 2C shows that the measured SBS instability threshold increased rapidly as  $L_{\rm eff}$  decreased (blue crosses). The blue curve shows that SBS threshold scaled inversely with  $L_{\rm eff}$ , as expected from our theory [see the supplementary materials, section 2 (17)]. To illustrate the enhancement by multimode excitation, the green circles show the estimated thresholds with FM-only excitation at fiber lengths corresponding to experimental values. At the shortest length  $L_{\rm eff}=3.7$  m, the measured SBS instability threshold reached 503 W, ~5 times higher than the FM-only threshold.

## **Output beam shaping**

All data points in Fig. 2C were taken with the output beam focused to a chosen spot outside of the distal facet of the MMF by optimizing the input phase front with the SLM [see the materials and methods (17)]. The inset in Fig. 2C is an optical image of focal spot taken at 173 W output signal power. With phase-only modulation of the input signal, 76% of total output power was concentrated within the focal area. We obtained similar focusing efficiencies at higher powers [fig. S7 (17)]. The near-field focusing of the output beam was achieved through interference of signal in many fiber modes, so the SBS instability threshold was enhanced by multimode excitation in the amplifier.

To control the output beam profile by input wavefront shaping, the signal bandwidth must be narrower than the spectral correlation width of a MMF amplifier. The latter characterizes how fast the output field pattern decorrelates with frequency detuning for a fixed input wavefront. Despite gain saturation and pump depletion in our MMF amplifier, its spectral correlation width barely changed from that of the passive MMF (50). With increasing fiber length, the spectral correlation width decreased, but even for the longest MMF of our amplifier, the correlation width exceeded 1 GHz, which is well above the signal bandwidth (see the next section). The amplified signal was spatially coherent; that is, the relative phase of output fields between any two positions was time invariant. Therefore, the speckle pattern created by multimode interference at any frequency within the signal bandwidth was almost identical, leading to the high-intensity contrast seen in the inset of Fig. 2A.

The spatial coherence of the amplified signal allowed us to generate the same output pattern, e.g., focusing to a chosen location, for all frequency components by imposing a single wavefront on the input beam. To measure the phase of the output field, we performed an interferometric experiment [see the materials and methods (17)]. The inset of Fig. 2C shows that the measured phase was constant across the focal spot, confirming diffraction-limited focusing.

To track axial evolution of a focal spot, we imaged the transverse intensity distribution at different axial planes. Three exemplary images are presented in Fig. 3, A to C, revealing that the spot radius increases

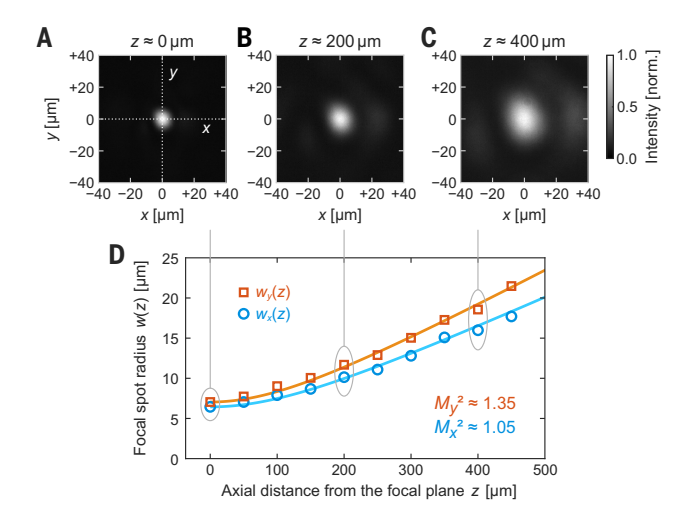


Fig. 3. Beam propagation factor of a focal spot at the MMF amplifier output. (A) Intensity profile of a diffraction-limited spot created 300  $\mu$ m from the MMF distal facet by shaping phase front of input signal; 76% of total output power was concentrated inside the focal area. (B and C) Output beam profiles recorded at axial distance  $z\approx 200~\mu$ m (B) and 400  $\mu$ m (C) from the focal plane, respectively. (D) Focal spot radii along x and y axes (perpendicular to fiber axis z),  $w_x$  and  $w_y$ , increased with axial distance z. Squares and circles mark experimental data, solid curves represent the fit with Eq. 3 that gives  $M_x^2\approx 1.05$  and  $M_y^2\approx 1.35$ .

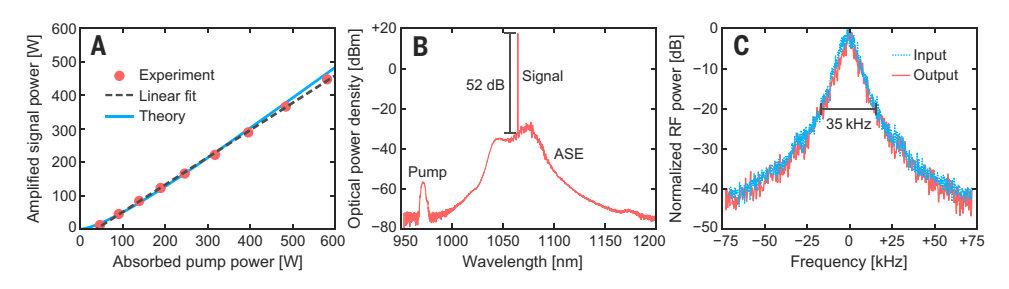


Fig. 4. High-power MMF amplifier with narrow linewidth. The fiber core diameter was 42  $\mu$ m and the effective length  $L_{\rm eff}$  was 3.7  $\mu$ m. (A) Amplified signal power as a function of absorbed pump power gives a slope efficiency of 82%. Red circles are experimental data, black dashed line is a linear fit of data, and blue curve is from our theoretical model. (B) Optical spectrum of amplifier output at 453 W power showing the amplified signal peak at 1064 nm on top of a broad amplified ASE band. The signal-to-ASE peak ratio was 52 dB. The small peak centered at 971 nm is from the residual pump. (C) Heterodyne spectra for input (blue) and output (red) signals of the MMF amplifier at an output signal power of 503 W. The sweep time was 41 ms. Full width at -20 dB of maximum was 35 kHz for both input and output signals, indicating no detectable spectral broadening by the MMF amplifier. After subtracting the reference linewidth, the 20-dB width of input/output signal was 18 kHz.

with axial distance z from the focal plane. We extracted the intensity profiles in the x and y axes and fit them with a Gaussian envelope to obtain the spot radius  $w_x$  and  $w_y$  [see the materials and methods (17)]. Figure 3D shows the growth of  $w_x$  and  $w_y$  with z. We fit the z dependence as follows:

$$w(z) = w(0)\sqrt{1 + \left(\frac{M^2 \lambda_{\rm S} z}{\pi n [w(0)]^2}\right)^2} \tag{3}$$

where w(0) is the focused spot radius at the focal plane (z=0),  $\lambda_{\rm S}$  is the signal wavelength in vacuum, and  $n\approx 1.45$  is the refractive index of the glass endcap in which the output beam is focused and further propagates. Equation 3 fits the data well and gives the beam propagation factors  $M_x{}^2\approx 1.05$  and  $M_y{}^2\approx 1.35$ .

## **Efficiency and linewidth**

We further characterized the performance of our high-power MMF amplifier with the shortest  $L_{\rm eff}=3.7~\mu m$ . First, we measured the output signal power and residual pump power. The power of the amplified signal is given by the difference between input and output signal power,  $P_S^{(\rm amp)}=P_S^{(\rm out)}-P_S^{(\rm in)}$ . The absorbed pump power was obtained by subtracting the residual pump power at the amplifier output from the pump power launched into the MMF,  $P_P^{(\rm abs)}=P_P^{(\rm in)}-P_P^{(\rm out)}$ . Figure 4A shows that  $P_S^{(\rm amp)}$  increased almost linearly with  $P_P^{(\rm abs)}$ . A linear fitting gives a slope efficiency of 82%. The experimental data agreed with the theoretical prediction of our model.

We also measured the output spectrum of the MMF amplifier with an optical spectrum analyzer. In Fig. 4B, the signal appears as a narrow peak at  $\lambda_S=1064$  nm. It sits on top of a broad amplified spontaneous emission (ASE) band. The peak ratio of amplified signal to ASE was 52 dB.

The signal linewidth, which was too narrow to be resolved by the optical spectrum analyzer, was measured by a heterodyne interferometer [see the materials and methods (*17*)]. Figure 4C shows the heterodyne peak resulting from beating of the amplified signal and a reference (red curve). The full width at –20 dB of the maximum was  $\Delta\nu_M=35$  kHz. Subtracting the reference width of  $\Delta\nu_R=17$  kHz (fig. S6), the 20-dB width of the output signal was  $\Delta\nu_S=\Delta\nu_M-\Delta\nu_R=18$  kHz, corresponding to a Lorentzian line of 3-dB bandwidth (full width at half maximum) ~1 kHz.

For comparison, we measured the linewidth of input signal to the MMF amplifier using the same method. As shown by the blue curve in Fig. 4C, the input signal had nearly identical width as the output (red curve), so optical wavefront shaping and coherent multimode amplification do not cause detectable spectral broadening of the signal. As mentioned earlier, a common approach to mitigating SBS in SMF

amplifiers is by broadening the input signal linewidth to tens of gigahertz. In our scheme, the 3-dB signal linewidth was six orders of magnitude narrower, and thus the temporal coherence length was six orders of magnitude longer in the MMF amplifier.

### **Discussion and conclusions**

Input wavefront shaping allowed us to simultaneously mitigate SBS in the MMF amplifier and control the output beam profile. Although an SLM placed at the fiber amplifier output end could shape the amplified beam and allow another SLM at the input end to optimize multimode excitation for maximal SBS suppression (50), we chose here to shape the low-power seed to avoid high-power handling. In the current experiment, phase-only modulation of the input wavefront

limited output focusing efficiency such that ~20 to 30% of power was outside of the focal spot. Complete focusing can be achieved with both amplitude and phase modulation of the input signal (35). Full-field modulation will also generate an output beam with  $M^2$  closer to unity (50). In addition to output focusing, input wavefront shaping can generate different output profiles of the MMF amplifier, which will be useful for laser welding and material processing. Even in the presence of strong nonlinearity, gain saturation, and pump depletion, as long as the amplifier operates below the instability threshold, optimal input wavefront can be found by minimizing the difference between the measured output beam shape and the target (51). In this work, the spatial profile of a single linear polarization of the output beam was controlled by input wavefront shaping. Although the input signal was linearly polarized, polarization mixing in the MMF caused depolarization. However, it was possible to control output beam profiles for two orthogonal polarizations by shaping both input polarizations. This could be done by separating two orthogonal polarizations of the input signal and shaping their field patterns separately before combining them and coupling them to the MMF (50).

An instability-free increase of the power in a MMF amplifier beyond the level demonstrated here will be possible by enlarging the fiber core to further suppress SBS. Even if only the FM is excited, the SBS threshold will scale quadratically with the core diameter [see the supplementary materials, section 2 (17)]. With multimode excitation, Brillouin spectrum broadening was more pronounced, because additional modes could be excited in an MMF with a larger core, leading to higher enhancement of the SBS threshold. Although our scheme does not rely on specialty fibers, wavefront shaping can be applied to specialized MMFs with lower optical nonlinearity and to microstructured fibers with a large cross-section for higher-power operation.

More generally, our method can be extended to mitigating other detrimental nonlinear effects in high-power fiber amplifiers, such as transverse mode instability, stimulated Raman scattering, and modulation instability, and also to other types of high-power lasers, such as solid-state and semiconductor optical amplifiers. Our scheme of spatial and modal spread of the signal may be combined with a temporal stretch of optical pulses for high-peak-power amplification.

## REFERENCES AND NOTES

- 1. D. J. Richardson, J. Nilsson, W. A. Clarkson, J. Opt. Soc. Am. B 27, B63-B92 (2010).
- J. Nilsson, D. N. Payne, Science 332, 921–922 (2011).
- 3. C. Jauregui, J. Limpert, A. Tünnermann, Nat. Photonics 7, 861-867 (2013).
- M. N. Zervas, C. A. Codemard, *IEEE J. Sel. Top. Quantum Electron.* 20, 0904123 (2013).
- 5. D. Strickland, G. Mourou, Opt. Commun. 55, 447-449 (1985)

- 6. Y. Jeong, J. Sahu, D. Payne, J. Nilsson, Opt. Express 12, 6088-6092 (2004).
- 7. L. Huang et al., Appl. Opt. 56, 5412-5417 (2017).
- 8. F. Beier et al., Opt. Express 25, 14892-14899 (2017).
- 9. R. Sidharthan et al., Opt. Lett. 45, 3828–3831 (2020).
- 10. C. Dixneuf et al., Opt. Express 28, 10960-10969 (2020).
- 11. K.-J. Lim et al., Photon. Res. 8, 1599-1604 (2020).
- 12. Y. Midilli, B. Ortaç, J. Lightwave Technol. 38, 1915-1920 (2020).
- 13. Y. Chen et al., Chin. Opt. Lett. 22, 041404 (2024).
- J. W. Nicholson et al., in Proc. SPIE 12400, Fiber Lasers XX: Technology and Systems, 1240002 (8 March 2023) (SPIE, 2023); https://doi.org/10.1117/12.2649969.
- 15. M. Cui et al., IEEE Photonics J. 17, 1-7 (2025).
- 16. F. Stutzki et al., Opt. Lett. 36, 689-691 (2011).
- 17. Supplementary materials are available online.
- 18. A. Kobyakov, M. Sauer, D. Chowdhury, Adv. Opt. Photonics 2, 1-59 (2010).
- Y. Panbhiharwala, A. V. Harish, D. Venkitesh, J. Nilsson, B. Srinivasan, Opt. Express 26, 33409–33417 (2018).
- 20. A. Flores, C. Robin, A. Lanari, I. Dajani, Opt. Express 22, 17735-17744 (2014).
- 21. M. Steinke et al., IEEE J. Sel. Top. Quantum Electron. 24, 1-13 (2017).
- A. Buikema, F. Jose, S. J. Augst, P. Fritschel, N. Mavalvala, Opt. Lett. 44, 3833–3836 (2019).
- 23. P. D. Dragic, C.-H. Liu, G. C. Papen, A. Galvanauskas, in (CLEO). Conference on Lasers and Electro-Optics, 2005 (IEEE, 2005); https://doi.org/10.1109/CLEO.2005.202342.
- 24. A. Liu, Opt. Express 15, 977-984 (2007).
- 25. C. Robin, I. Dajani, B. Pulford, Opt. Lett. 39, 666-669 (2014).
- 26. L. Huang et al., Opt. Lett. 42, 1-4 (2017).
- 27. S. Hochheim et al., J. Lightwave Technol. 40, 2136-2143 (2021).
- 28. T. Hawkins et al., J. Opt. Soc. Am. B 38, F38-F49 (2021).
- 29. W. Jiang et al., Photonics 9, 518 (2022).
- 30. C. Shi et al., Front. Phys. 10, 982900 (2022).
- 31. C. Li et al., Chin. Opt. Lett. 21, 090002 (2023).
- 32. H. Cao, A. P. Mosk, S. Rotter, Nat. Phys. 18, 994-1007 (2022).
- 33. I. N. Papadopoulos, S. Farahi, C. Moser, D. Psaltis, Opt. Express 20, 10583-10590 (2012).
- A. M. Caravaca-Aguirre, E. Niv, D. B. Conkey, R. Piestun, Opt. Express 21, 12881–12887 (2013).
- 35. A. D. Gomes, S. Turtaev, Y. Du, T. Čižmár, Opt. Express 30, 10645-10663 (2022).
- 36. R. Florentin et al., Light Sci. Appl. 6, e16208 (2017).
- 37. R. Florentin, V. Kermene, A. Desfarges-Berthelemot, A. Barthelemy, *Opt. Express* 27, 32638–32648 (2019).
- 38. J. Montoya et al., Opt. Express 25, 27543-27550 (2017).
- 39. O. Tzang, A. M. Caravaca-Aguirre, K. Wagner, R. Piestun, Nat. Photonics 12, 368-374 (2018).
- 40. E. Deliancourt et al., Opt. Express 27, 17311-17321 (2019).

- 41. L. G. Wright, W. H. Renninger, D. N. Christodoulides, F. W. Wise, Optica 9, 824-841 (2022).
- 42. R. G. Harrison, J. S. Uppal, A. Johnstone, J. V. Moloney, Phys. Rev. Lett. 65, 167-170 (1990).
- 43. A. L. Gaeta, R. W. Boyd, Phys. Rev. A 44, 3205-3209 (1991).
- G. P. Agrawal, Nonlinear Fiber Optics (Academic Press, 4 ed., 2006); https://doi.org/10.1016/b978-0-12-369516-1.x5000-6.
- Y. Panbiharwala, A. Ghosh, J. Nilsson, D. Venkitesh, B. Srinivasan, in Proc. SPIE 10512, Fiber Lasers XV: Technology and Systems, 105122X (26 February 2018) (SPIE, 2018); https://doi.org/10.1117/12.2291462.
- 46. K. Wisal, S. C. Warren-Smith, C.-W. Chen, H. Cao, A. D. Stone, *Phys. Rev. X* 14, 031053 (2024).
- 47. C.-W. Chen et al., Nat. Commun. 14, 7343 (2023).
- 48. K. Wisal et al., Optica 11, 1663-1672 (2024).
- 49. K. Wisal, C.-W. Chen, H. Cao, A. D. Stone, APL Photonics 9, 066114 (2024).
- 50. S. Rothe et al., Opt. Commun. 577, 131405 (2025).
- 51. C.-W. Chen, K. Wisal, M. Fink, A. D. Stone, H. Cao, Nat. Phys. 21, 839-845 (2025).
- 52. S. Rothe *et al.*, Data for: Wavefront shaping enables high-power multimode fiber amplifier with output focus, Zenodo (2025); https://doi.org/10.5281/zenodo.16651538.

#### ACKNOWLEDGMENTS

We thank F. M. Ferreira, N. Bender, O. D. Miller, O. Henderson-Sapir, S. C. Warren-Smith, D. L. Smith, L. V. Nguyen, D. J. Ottaway, H. Ebendorff-Heidepriem, M. J. F. Digonnet, and J. Ballato for fruitful discussions; N. Bernardo and V. Bernardo at Yale University for technical assistance; and AFL, Thorlabs, Lightel, and NP Photonics for support. Funding: This work was supported by the Air Force Office of Scientific Research (AFOSR grant FA9550-24-1-0182 to H.C. and A.D.S.) and the German Research Foundation (DFG grant RO 7348/1-1 to S.R.). Author contributions: H.C. proposed the idea and initiated the project. S.R., C.-W.C., P.A., and K.L. designed and built the MMF amplifier system, performed the experiments in collaboration with M.E. and N.V, and analyzed the data in collaboration with K.W. under the supervision of H.C. K.W. developed the theory and numerical simulations under the supervision of A.D.S. S.R., C.-W.C., K.W., A.D.S., and H.C. wrote the manuscript with input from all authors. Competing interests: The authors declare no competing interests. Data and materials availability: All data needed to evaluate the conclusions in the study are present in the main text or the supplementary materials. The data for all figures are archived in Zenodo (52). License information: Copyright © 2025 the authors, some rights reserved; exclusive licensee American Association for the Advancement of Science. No claim to original US government works. https://www.science.org/about/science-licenses-journal-article-reuse

#### SUPPLEMENTARY MATERIALS

science.org/doi/10.1126/science.ady2226 Materials and Methods; Figs. S1 to S6; Tables S1 to S3; References (53–72)

Submitted 14 April 2025; accepted 13 August 2025

10.1126/science.ady2226